Simulating Colloids and Self-Propelled Particles with Fully Resolved Hydrodynamics Using the Smoothed Profile Method (SPM)

Ryoichi Yamamoto, John J. Molina, and Rei Tatsumi

Department of Chemical Engineering, Kyoto University, Kyoto 615-8510, Japan
E-mail: {*ryoichi, john, tatsumi*}*@cheme.kyoto-u.ac.jp*

The smoothed profile method (SPM) provides an efficient numerical scheme for coupling continuum fluid dynamics with moving dispersed particles using a smeared interface between the fluids and the particles. The SPM has been successfully applied to directly simulate several dynamical problems of colloidal dispersions in incompressible fluids, including those involving sedimentation, diffusion, coagulation, rheology, and tumbling motion in shear flow as well as electrophoresis in external electric fields. More recently, the SPM was extended to two important problems. The first extension simulates colloidal particles in compressible host fluids, whereas the second extension simulates self-propelled swimming particles. A comprehensive summary of SPM is provided in this paper.

1 Introduction

Interparticle interactions in colloidal dispersions mainly consist of thermodynamic potential interactions as well as hydrodynamic interactions. Whereas the former applies to both static and dynamic situations, the latter only applies to dynamic situations. Although thermodynamic interactions in static situations have been studied extensively and are treated as effective interactions, the nature of dynamic interactions is poorly understood. Because hydrodynamic interactions are essentially long-range, many-body effects, they are extremely difficult to study using analytical means alone. Numerical simulations can be used to investigate the role of hydrodynamic interactions in colloidal dynamics.

Several numerical methods have been developed to simulate the dynamics of colloidal dispersions. Two of the most well-known methods include Stokesian dynamics[1] and the Eulerian–Lagrangian method[2]. The former is the most widely used method because of its proper treatment of hydrodynamic interactions between spherical particles in a Newtonian fluid at zero Reynolds number. Furthermore, it can be implemented as a $O(N)$ scheme for N particles by utilizing the fast multi-pole method[3]. However, it is not easy to address dense dispersions and dispersions consisting of non-spherical particles by means of Stokesian dynamics due to the complicated mathematical structures used in Stokesian dynamics. In contrast, the Eulerian–Lagrangian method is a very natural and sensible approach for stimulating solid particles. It is possible to apply this method to dispersions consisting of many particles with different shapes. However, numerical efficiencies arise from the following concerns: i) the re-construction of irregular meshes according to the temporal particle position is necessary for every simulation step, and ii) the Navier–Stokes equation must be solved with boundary conditions imposed on the surfaces of all colloidal particles. Thus, these computational demands are particularly cumbersome for systems involving many particles, even if the shapes are all spherical.

To overcome problems arising from the particle-fluid interface in the Eulerian–Lagrangian method, we have developed an efficient direct numerical simulation (DNS) method for colloidal dispersions. This method was named the "smoothed profile method (SPM)" because the original sharp interface between the colloids and solvent is replaced by a smeared out, smoothed interface with a finite thickness[4–20]. This simple modification greatly improves the resulting quality of the of numerical computations in comparison with the original Eulerian–Lagrangian method for the following reasons:

1. Regular fixed Cartesian coordinates can be used for many particle systems by defining a particle shape instead of providing boundary-fitted coordinates. The particle-fluid interface has a finite volume ($\propto \pi a^{d-1}\xi$, with a and d as the particle radius and system dimension) supported by multiple grid points. Thus, the round particles can be treated in a fixed Cartesian coordinates without any difficulties. The simulation scheme is thus free from the mesh re-construction problem that significantly suppresses the computational efficiency of the Eulerian–Lagrangian method. In addition, the simple Cartesian coordinate enables the use of periodic boundary conditions as well as fast Fourier transformations (FFT).

2. At the particle-fluid interfaces, the velocity component in the direction normal to the interface of the host fluid must be equal to that of the particle. In the Eulerian–Lagrangian method, this non-penetration condition is imposed by the Navier–Stokes equation as the boundary condition defined for the particle-fluid interface. In the SPM, however, this condition is automatically satisfied by an incompressibility condition on the entire domain.

3. The computational demands for this method include sensitivity to the number of grid points (volume of the total system). Nevertheless, because the method is insensitive to the number of particles, it is suitable for simulating dense colloidal dispersions.

The SPM has been successfully used to directly simulate various dynamical problems of colloidal dispersion in incompressible fluids, including sedimentation[20], diffusion[9,12,13], coagulation[8,19], rheology[11,14,17], tumbling motion in shear flow[15], and electrophoresis in external electric fields[7,10]. Several simulation methods similar in spirit to the SPM have also been proposed in recent publications[22–25]. A comprehensive summary of SPM is provided in this study including the recent key extensions for stimulating colloidal particles in compressible host fluids[18] and also for stimulating the self-propelled swimming of particles[21].

2 Colloids in Incompressible Fluids

2.1 Working Equations

The motion of the host fluid is determined by the Navier-Stokes equation with the following incompressibility condition:

$$\nabla \cdot \boldsymbol{u}_f = 0 \tag{1}$$

$$\rho \left(\partial_t + \boldsymbol{u}_f \cdot \nabla\right) \boldsymbol{u}_f = \nabla \cdot \boldsymbol{\sigma} \tag{2}$$

where ρ is the total mass density of the fluid, $\boldsymbol{u}_f$ is the host fluid velocity field, $\boldsymbol{\sigma}$ is the stress tensor

$$\boldsymbol{\sigma} = -p\boldsymbol{I} + \boldsymbol{\sigma}' \tag{3}$$

$$\boldsymbol{\sigma}' = \eta\left[\nabla \boldsymbol{u}_f + (\nabla \boldsymbol{u}_f)^{\mathrm{t}}\right] \tag{4}$$

and η is the shear viscosity of the fluid. Consider a mono-disperse system containing N-spherical particles with a radius a, mass M_p, and moment of inertia $\boldsymbol{I}_p = 2/5 M_p a^2 \boldsymbol{I}$ (with $\boldsymbol{I}$ the unit tensor). The evolution of colloids is described by the Newton-Euler equations[28],

$$\begin{aligned} \dot{\boldsymbol{R}}_i &= \boldsymbol{V}_i & \dot{\boldsymbol{Q}}_i &= \boldsymbol{Q}_i \,\mathrm{skew}\,(\boldsymbol{\Omega}_i) \\ M_p \dot{\boldsymbol{V}}_i &= \boldsymbol{F}_i^{\mathrm{H}} + \boldsymbol{F}_i^{\mathrm{C}} + \boldsymbol{F}_i^{\mathrm{ext}} & \boldsymbol{I}_p \cdot \dot{\boldsymbol{\Omega}}_i &= \boldsymbol{N}_i^{\mathrm{H}} + \boldsymbol{N}^{\mathrm{ext}} \end{aligned} \tag{5}$$

where $\boldsymbol{R}_i$ and $\boldsymbol{V}_i$ denote the centre of mass positions and the velocity of the particle i, respectively, and $\boldsymbol{Q}_i$ is the orientation matrix[b]. Hence, $\boldsymbol{\Omega}_i$ the angular velocity and skew $(\boldsymbol{\Omega}_i)$ is the skew-symmetric angular velocity matrix:

$$\mathrm{skew}(\boldsymbol{\Omega}_i) = \begin{pmatrix} 0 & -\Omega_i^z & \Omega_i^y \\ \Omega_i^z & 0 & -\Omega_i^x \\ -\Omega_i^y & \Omega_i^x & 0 \end{pmatrix} \tag{6}$$

The forces on the particles are comprised of hydrodynamic contributions arising from fluid-particle interactions $\boldsymbol{F}^{\mathrm{H}}$, colloid-colloid interactions due to the core particle potential $\boldsymbol{F}^{\mathrm{C}}$ (which prevents particle overlap), and a possible external field contribution $\boldsymbol{F}^{\mathrm{ext}}$ (such as gravity). Likewise, the torques on the particles can be divided into a hydrodynamic $\boldsymbol{N}^{\mathrm{H}}$ and an external contribution $\boldsymbol{N}^{\mathrm{ext}}$ (for simplicity, the particle-particle interactions are assumed to be described by a radial potential). Subsequently, we consider buoyancy-neutral particles, for which $\boldsymbol{F}^{\mathrm{ext}} = \boldsymbol{N}^{\mathrm{ext}} = 0$. Finally, the conservation of momentum between the fluid and the particles implies the following hydrodynamic force and torque on the i-th particle:

$$\boldsymbol{F}_i^{\mathrm{H}} = \int \mathrm{d}\boldsymbol{S}_i \cdot \boldsymbol{\sigma} \tag{7}$$

$$\boldsymbol{N}_i^{\mathrm{H}} = \int (\boldsymbol{x} - \boldsymbol{R}_i) \times (\mathrm{d}\boldsymbol{S}_i \cdot \boldsymbol{\sigma}) \tag{8}$$

where $\int \mathrm{d}\boldsymbol{S}_i$ indicates an integral over the surface of the particle. In addition, thermal fluctuations can be introduced by adding a random stress tensor $\boldsymbol{s}$in Eq. 3, that satisfies the fluctuation-dissipation relation:[26]

$$\langle s_{ik}(\boldsymbol{x}, t) s_{jl}(\boldsymbol{x}', t')\rangle = 2k_B T\eta(\delta_{ij}\delta_{kl} + \delta_{il}\delta_{kj})\delta(\boldsymbol{x} - \boldsymbol{x}')\delta(t - t'), \tag{9}$$

where k_B is the Boltzmann constant, T is the temperature. Alternatively, it is also possible to introduce thermal fluctuations by adding Langevin random forces and torque to Eq. 5[9,11–13].

[b]For numerical stability, we use quaternion instead of rotation matrices to represent the rigid body dynamics of the particles.

2.2 Simulation Procedure for Incompressible Fluids

We now present the computational algorithm used to simulate the motion of spherical particles using the SPM. We require that all field variables are defined over the entire computational domain (fluid + particle). The concentration field for the colloids is described as follows:

$$\phi(\boldsymbol{x},t) = \sum_{i=1}^{N} \phi_i(\boldsymbol{x},t), \tag{10}$$

where $\phi_i \in [0,1]$ is the smooth profile field of particle i. This field is defined as unity within the particle domain, as zero in the fluid domain, and as a smooth interpolation between the two extremes within the interface region. Several possible mathematical forms exist for $\phi_i(\boldsymbol{x})$, however, we adopted the following definition of ϕ_i:

$$\phi_i(\boldsymbol{x}) = g(|\boldsymbol{x} - \boldsymbol{R}_i|), \tag{11}$$

$$g(x) = \frac{h((a+\xi/2)-x)}{h((a+\xi/2)-x) + h(x-(a-\xi/2))}, \tag{12}$$

$$h(x) = \begin{cases} \exp\left(-\Delta^2/x^2\right) & x \geq 0, \\ 0 & x < 0. \end{cases} \tag{13}$$

where a, ξ, and Δ are the radius of the particle, the interfacial thickness, and lattice spacing, respectively. The particle velocity field is defined in a similar fashion:

$$\phi \boldsymbol{u}_p(\boldsymbol{x},t) = \sum_{i=1}^{N} \left\{ \boldsymbol{V}_i(t) + \boldsymbol{\Omega}_i(t) \times \boldsymbol{r}_i(t) \right\} \phi_i(\boldsymbol{x},t) \tag{14}$$

with $\boldsymbol{r}_i = \boldsymbol{x} - \boldsymbol{R}_i$, which allows one to define the total fluid velocity field using the following expression:

$$\boldsymbol{u}(\boldsymbol{x},t) \equiv (1-\phi)\boldsymbol{u}_f + \phi \boldsymbol{u}_p \tag{15}$$

where the incompressibility condition is satisfied over the entire domain $\nabla \cdot \boldsymbol{u} = 0$. The evolution equation for $\boldsymbol{u}$ is then derived assuming momentum-conservation between fluid and particles[6,10]

$$\rho \left(\partial_t + \boldsymbol{u} \cdot \nabla \right) \boldsymbol{u} = \nabla \cdot \boldsymbol{\sigma} + \rho \phi \boldsymbol{f}_p \tag{16}$$

where $\phi \boldsymbol{f}_p$ represents the force density field needed to maintain rigidity constraints on the particle velocity field.

We use a fractional step approach to update the total velocity field. Let $\boldsymbol{u}^n$ be the field at time $t_n = nh$ (h is the time interval).

i) We first solve for advection and hydrodynamic viscous stress terms, and we then propagate the particle positions (orientations) using the current particle velocities,

which affords the following relation:

$$\boldsymbol{u}^* = \boldsymbol{u}^n + \int_{t_n}^{t_n+h} \mathrm{d}s\, \nabla \cdot \left[\frac{1}{\rho}\left(-p^*\boldsymbol{I} + \boldsymbol{\sigma}'\right) - \boldsymbol{u}\boldsymbol{u}\right] \tag{17}$$

$$\boldsymbol{R}_i^{n+1} = \boldsymbol{R}_i^n + \int_{t_n}^{t_n+h} \mathrm{d}s\, \boldsymbol{V}_i \tag{18}$$

$$\boldsymbol{Q}_i^{n+1} = \boldsymbol{Q}_i^n + \int_{t_n}^{t_n+h} \mathrm{d}s\, \boldsymbol{Q}_i \mathrm{skew}\left(\boldsymbol{\Omega}_i\right) \tag{19}$$

where the pressure term p^* in Eq. 17 is determined by the incompressibility condition $\nabla \cdot \boldsymbol{u}^* = 0$. The remaining updating procedure imposes a rigidity constraint on the velocity field.

ii) The hydrodynamic force and torque exerted by the fluid on the colloids is determined by assuming momentum conservation. The time integrated hydrodynamic force and torque over a period h are equal to the momentum exchange over the particle domain

$$\left[\int_{t_n}^{t_n+h} \mathrm{d}s\, \boldsymbol{F}_i^{\mathrm{H}}\right] = \int \mathrm{d}\boldsymbol{x}\, \rho\phi_i^{n+1}\left(\boldsymbol{u}^* - \boldsymbol{u}_p^n\right) \tag{20}$$

$$\left[\int_{t_n}^{t_n+h} \mathrm{d}s\, \boldsymbol{N}_i^{\mathrm{H}}\right] = \int \mathrm{d}\boldsymbol{x}\, \left[\boldsymbol{r}_i^{n+1} \times \rho\phi_i^{n+1}\left(\boldsymbol{u}^* - \boldsymbol{u}_p^n\right)\right] \tag{21}$$

Based on this and other forces acting on the colloids, the particles velocities are updated as follows:

$$\boldsymbol{V}_i^{n+1} = \boldsymbol{V}_i^n + M_p^{-1}\left[\int_{t_n}^{t_n+h} \mathrm{d}s\, \boldsymbol{F}_i^{\mathrm{H}}\right] + M_p^{-1}\left[\int_{t_n}^{t_n+h} \mathrm{d}s\, \left(\boldsymbol{F}_i^{\mathrm{C}} + \boldsymbol{F}_i^{\mathrm{ext}}\right)\right] \tag{22}$$

$$\boldsymbol{\Omega}_i^{n+1} = \boldsymbol{\Omega}_i^n + \boldsymbol{I}_p^{-1} \cdot \left[\int_{t_n}^{t_n+h} \mathrm{d}s\, \boldsymbol{N}_i^{\mathrm{H}}\right] + \boldsymbol{I}_p^{-1} \cdot \left[\int_{t_n}^{t_n+h} \mathrm{d}s\, \boldsymbol{N}_i^{\mathrm{ext}}\right] \tag{23}$$

iii) Finally, the resulting particle velocity field $\phi^{n+1}\boldsymbol{u}_p^{n+1}$ is enforced on the total velocity field as follows:

$$\boldsymbol{u}^{n+1} = \boldsymbol{u}^* + \left[\int_{t_n}^{t_n+h} \mathrm{d}s\, \phi\boldsymbol{f}_p\right] \tag{24}$$

$$\left[\int_{t_n}^{t_n+h} \mathrm{d}s\, \phi\boldsymbol{f}_p\right] = \phi^{n+1}\left(\boldsymbol{u}_p^{n+1} - \boldsymbol{u}^*\right) - \frac{h}{\rho}\nabla p_{\mathrm{p}} \tag{25}$$

wherein the pressure is due to the rigidity constraint obtained from the incompressibility condition $\nabla \cdot \boldsymbol{u}^{n+1} = 0$. The total pressure field is thus obtained as $p = p^* + p_{\mathrm{p}}$.

The above procedure defines the consistent time-propagation, $\{\boldsymbol{u}^n; \boldsymbol{R}_i^n, \boldsymbol{Q}_i^n, \boldsymbol{\Omega}_i^n\} \rightarrow \{\boldsymbol{u}^{n+1}; \boldsymbol{R}_i^{n+1}, \boldsymbol{Q}_i^{n+1}, \boldsymbol{\Omega}_i^{n+1}\}$, to simulate colloidal particles in incompressible fluids.

3 Colloids in Compressible Fluids

3.1 Working Equations

The hydrodynamic equations consist of three conservation laws concerning mass, momentum, and energy. The conservation equations of mass and momentum for incompressible fluids are described by the following:

$$\frac{\partial \rho}{\partial t} + \nabla \cdot \boldsymbol{m} = 0, \tag{26}$$

$$\frac{\partial \boldsymbol{m}}{\partial t} + \nabla \cdot (\boldsymbol{m}\boldsymbol{u}) = \nabla \cdot \boldsymbol{\sigma} + \rho\phi \boldsymbol{f}_p, \tag{27}$$

where $\boldsymbol{m}(\boldsymbol{r}, t) = \rho(\boldsymbol{r}, t)\boldsymbol{u}(\boldsymbol{x}, t)$ is the momentum density field. We consider a compressible Newtonian fluid, and the stress tensor is described as follows:

$$\boldsymbol{\sigma} = -p\boldsymbol{I} + \eta[\nabla \boldsymbol{u} + (\nabla \boldsymbol{u})^{\mathrm{t}}] + \left(\eta_v - \frac{2}{3}\eta\right)(\nabla \cdot \boldsymbol{u})\boldsymbol{I}, \tag{28}$$

where $p(\boldsymbol{r}, t)$ is the pressure, η is the shear viscosity, and η_v is the bulk viscosity. A body force $\rho\phi \boldsymbol{f}_p$ is also added to satisfy the rigidity of the particles. Additionally, we assume a barotropic fluid described by $p = p(\rho)$, with a pressure gradient that is proportional to the density:

$$\nabla p = c^2 \nabla \rho, \tag{29}$$

where c is the speed of sound in the fluid. Eqs. 26-29 are closed to variables ρ, $\boldsymbol{m}$, and p; therefore, energy conservation does not need to be considered for barotropic fluids.

The motion of the dispersed particles is governed by Newton-Euler equations of motion Eq. 5. The effect of thermal fluctuations on the particles dynamics is important when the particle size is on the order of a micrometer or smaller. Fluctuations were introduced using a random stress tensor $\boldsymbol{s}$, which is added to the stress tensor Eq. 28. The random stress is a stochastic variable satisfying the fluctuation-dissipation relation[26]:

$$\langle s_{ij}(\boldsymbol{r}, t) s_{kl}(\boldsymbol{r}', t') \rangle = 2k_B T \eta_{ijkl} \delta(\boldsymbol{r}' - \boldsymbol{r}) \delta(t' - t), \tag{30}$$

and

$$\eta_{ijkl} = \eta(\delta_{ik}\delta_{jl} + \delta_{il}\delta_{jk}) + \left(\eta_v - \frac{2}{3}\eta\right)\delta_{ij}\delta_{kl}. \tag{31}$$

Brownian motion of the dispersed particles is induced by the random stresses acting on the fluid. Thermal fluctuations can be introduced using the Langevin approach, wherein random forces are exerted on the particles[9,11–13]. However, this approach does not accurately represent the short-time dynamics of the system because the autocorrelation time of the hydrodynamic force acting on the particles is neglected. Therefore, the fluctuating hydrodynamics approach is more appropriate for investigating dynamics at a time scale of sound propagation.

3.2 Simulation Procedure for Compressible Fluids

In this section, the time-discretized evolution of the equations is derived for colloidal dispersions in compressible fluids. The time evolution of the fluid is determined using the following steps:

i) The mass and momentum density changes associated with sound propagation are calculated using the following equations:

$$\rho^{n+1} = \rho^n - \int_{t_n}^{t_n+h} \mathrm{d}s\, \nabla \cdot \boldsymbol{m}, \tag{32}$$

$$\boldsymbol{m}^* = \boldsymbol{m}^n - c^2 \int_{t_n}^{t_n+h} \mathrm{d}s\, \nabla \rho. \tag{33}$$

When we assume a periodic boundary condition and use the Fourier spectral method, a semi-implicit scheme becomes feasible[27]. This situation eliminates restrictions on time increments with a small compressibility factor ε.

ii) The time evolution of the advection and viscous diffusion terms are calculated using the following equations:

$$\boldsymbol{m}^{**} = \boldsymbol{m}^* + \int_{t_n}^{t_n+h} \mathrm{d}s\, \nabla \cdot (\boldsymbol{\sigma}' - \boldsymbol{m}\boldsymbol{u}), \tag{34}$$

where $\boldsymbol{\sigma}'$ is the dissipative stress defined in Eq. 3.

iii) In concert with the advection of the particle domain, the position (orientation) of each dispersed particle evolves according to the following equations:

$$\boldsymbol{R}_i^{n+1} = \boldsymbol{R}_i^n + \int_{t_n}^{t_n+h} \mathrm{d}s\, \boldsymbol{V}_i \tag{35}$$

$$\boldsymbol{Q}_i^{n+1} = \boldsymbol{Q}_i^n + \int_{t_n}^{t_n+h} \mathrm{d}s\, \boldsymbol{Q}_i \mathrm{skew}\left(\boldsymbol{\Omega}_i\right). \tag{36}$$

iv) The hydrodynamic force and torque are derived by considering the conservation of momentum. The time-integrated hydrodynamic force and torque are computed using the following equations:

$$\int_{t_n}^{t_n+h} \mathrm{d}s\, \boldsymbol{F}_i^H = \int \mathrm{d}\boldsymbol{x}\, \phi_i^{n+1}(\boldsymbol{m}^{**} - \rho^{n+1}\boldsymbol{u}_p^n), \tag{37}$$

$$\int_{t_n}^{t_n+h} \mathrm{d}s\, \boldsymbol{N}_i^H = \int \mathrm{d}\boldsymbol{x}\, [(\boldsymbol{r} - \boldsymbol{R}_i^{n+1}) \times \phi_i^{n+1}(\boldsymbol{m}^{**} - \rho^{n+1}\boldsymbol{s}_p^n)]. \tag{38}$$

With these and other forces acting on the particles, the translational and rotational velocities of each dispersed particle evolve according to the following equations:

$$\boldsymbol{V}_i^{n+1} = \boldsymbol{V}_i^n + M_p^{-1} \int_{t_n}^{t_n+h} \mathrm{d}s\, (\boldsymbol{F}_i^H + \boldsymbol{F}_i^C), \tag{39}$$

$$\boldsymbol{\Omega}_i^{n+1} = \boldsymbol{\Omega}_i^n + \boldsymbol{I}_p^{-1} \cdot \int_{t_n}^{t_n+h} \mathrm{d}s\, \boldsymbol{N}_i^H. \tag{40}$$

v) The updated velocity of the particle region is imposed on the velocity field as the volume force $\rho\phi\boldsymbol{f}_p$.

$$\boldsymbol{m}^{n+1} = \boldsymbol{m}^{**} + \int_{t_n}^{t_n+h} \mathrm{d}s\, \rho\phi\boldsymbol{f}_p, \tag{41}$$

$$\int_{t_n}^{t_n+h} \mathrm{d}s\, \rho\phi\boldsymbol{f}_p = \phi^{n+1}(\rho^{n+1}\boldsymbol{u}_p^{n+1} - \boldsymbol{m}^{**}). \tag{42}$$

In the case of an incompressible fluid, the pressure is spontaneously determined by the solenoid condition of the velocity field. In contrast, in this case, the pressure and mass density variations are independent of the velocity field.

The above procedure defines the consistent time-propagation, $\{\rho^n, \boldsymbol{m}^n; \boldsymbol{R}_i^n, \boldsymbol{Q}_i^n, \boldsymbol{\Omega}_i^n\} \to \{\rho^{n+1}, \boldsymbol{m}^{n+1}; \boldsymbol{R}_i^{n+1}, \boldsymbol{Q}_i^{n+1}, \boldsymbol{\Omega}_i^{n+1}\}$, to simulate colloidal particles in compressible fluids.

4 Self-Propelled Particles

4.1 Squirmer Model

We consider a simple model of self-propelled spherical swimmers, originally introduced by Lighthill[29] and later extended by Blake[30], which move due to a self-generated surface-tangential velocity $\boldsymbol{u}^s$. This specific mechanism was proposed as a model for an ideal ciliate particle, in which the synchronized beating of the cilia at the surface gives rise to net motion in the absence of any external fields. If one assumes that the displacements of this cilia envelope are purely tangential, then the effective (time-averaged) slip velocity for these *squirmers* is described by the following equation[30]:

$$\boldsymbol{u}^s(\hat{\boldsymbol{r}}) = \sum_{n=1}^{\infty} \frac{2}{n\,(n+1)} B_n\, (\hat{\boldsymbol{e}}\cdot\hat{\boldsymbol{r}}\hat{\boldsymbol{r}} - \hat{\boldsymbol{e}})\, P_n'\,(\hat{\boldsymbol{e}}\cdot\hat{\boldsymbol{r}}) \tag{43}$$

where $\hat{\boldsymbol{e}}$ is the squirmer's fixed swimming axis (*i.e.*, we consider that each squirmer carries with it a fixed coordinate system that determines its preferred swimming direction at each instant), $\hat{\boldsymbol{r}}$ is a unit vector from the particle centre to a point on the surface, P_n' is the derivative of the n-th order Legendre polynomial, and B_n is the amplitude of the corresponding mode.

When all squirming modes higher than three are neglected, $B_n = 0\,(n \geq 3)$, the following simple expression for the surface tangential velocity as a function of polar angle $\theta = \cos^{-1}(\hat{\boldsymbol{r}}\cdot\hat{\boldsymbol{e}})$, is obtained:

$$\boldsymbol{u}^s(\theta) = B_1 \left(\sin\theta + \frac{\alpha}{2}\sin 2\theta\right) \tag{44}$$

where $\alpha = B_2/B_1$ determines whether the swimmer is a pusher ($\alpha < 0$) or a puller ($\alpha > 0$). A schematic representation of the flow profile generated by these two types of swimmers is provided in Fig. 1. An example of the former include spermatozoa and most bacteria, whereas the latter includes unicellular algae *Chlamydomonas*. Although the squirmer model we adopt does not include a detailed propulsion mechanism, it is capable of distinguishing between pushers/pullers and provides an adequate approximation for the far-field flow profile generated by these swimmers.

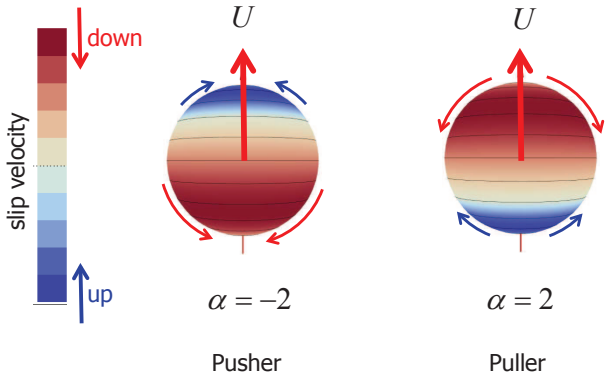

Figure 1. Schematic representation of the flow profiles generated by a pusher (left) and a puller (right). In both cases, the particle's swimming direction is towards the top of the page.

For Newtonian fluids, which is the only case considered here, the swimming speed U of the squirmer is determined uniquely by the first mode B_1, irrespective of the size of the particle, as $U = 2/3B_1$, while the second mode gives the strength of the stresslet[31,32]. In the Stokes regime, the velocity field generated by a single such squirmer was solved analytically by Ishikawa et al.[31], providing the following expression in the laboratory frame (fluid at rest far away from the particle):

$$\boldsymbol{u}(\boldsymbol{r}) = B_1 \frac{a^2}{r^2}\left[\frac{a}{r}\left(\frac{2}{3}\hat{\boldsymbol{e}} + \sin\theta\,\hat{\boldsymbol{\theta}}\right) + \frac{\alpha}{2}\left\{\left(\frac{a^2}{r^2} - 1\right)\left(3\cos^2\theta - 1\right)\hat{\boldsymbol{r}} + \frac{a^2}{r^2}\sin 2\theta\,\hat{\boldsymbol{\theta}}\right\}\right] \tag{45}$$

where a is the radius of the particle. Notice that for neutral swimmers ($\alpha = 0$), the velocity field decays as r^{-3}, whereas for pushers/pullers ($\alpha \neq 0$), the velocity field decays as r^{-2}. In contrast, the velocity field for a sedimenting particle (or a particle experiencing a net body force) decays as r^{-1} [33]. This observation will have important consequences on the hydrodynamic interactions describing suspensions of swimmers.

4.2 Simulation Procedure for Squirmers

We now present the computational algorithm used to simulate the motion of spherical particles, with a given surface tangential slip velocity $\boldsymbol{u}^s$ using the SPM. The evolution equation for $\boldsymbol{u}$ is then derived by assuming momentum-conservation between the fluid and particles[6,10]

$$\rho\left(\partial_t + \boldsymbol{u}\cdot\nabla\right)\boldsymbol{u} = \nabla\cdot\boldsymbol{\sigma} + \rho\phi\boldsymbol{f}_p + \rho\boldsymbol{f}_{sq} \tag{46}$$

where $\phi\boldsymbol{f}_p$ represents the force density field needed to maintain the rigidity constraint on the particle velocity field and $\boldsymbol{f}_{sq}$ is the force density field generated by the squirming motion of the particles. The motion of the dispersed particles is governed by Newton-Euler equations of motion Eq. 5.

We use the fractional step approach to update the total velocity field.

i) We first solve for the advection and hydrodynamic viscous stress terms, and we then propagate the particle positions (orientations) using the current particle velocities. This operation yields the following results:

$$\boldsymbol{u}^* = \boldsymbol{u}^n + \int_{t_n}^{t_n+h} \mathrm{d}s \, \nabla \cdot \left[\frac{1}{\rho} \left(-p^* \boldsymbol{I} + \boldsymbol{\sigma}' \right) - \boldsymbol{u}\boldsymbol{u} \right] \tag{47}$$

$$\boldsymbol{R}_i^{n+1} = \boldsymbol{R}_i^n + \int_{t_n}^{t_n+h} \mathrm{d}s \, \boldsymbol{V}_i \tag{48}$$

$$\boldsymbol{Q}_i^{n+1} = \boldsymbol{Q}_i^n + \int_{t_n}^{t_n+h} \mathrm{d}s \, \boldsymbol{Q}_i \mathrm{skew}\left(\boldsymbol{\Omega}_i \right) \tag{49}$$

where the pressure term p^* in Eq. 47 is determined by the incompressibility condition $\nabla \cdot \boldsymbol{u}^* = 0$. The remaining updating procedure applies to the slip condition at the particle boundary as well as the rigidity constraint on the velocity field.

ii) We now consider the momentum change needed to maintain the slip velocity at the surface of each of the squirmers, where the slip profile $\boldsymbol{u}^s$ is imposed with respect to the particle velocities $\{\boldsymbol{V}_i'; \boldsymbol{\Omega}_i'\}$, using the previously updated positions and orientations orientations $\{\boldsymbol{R}_i^{n+1}; \boldsymbol{Q}_i^{n+1}\}$. We note that at this point we do not yet know the correct updated particle velocities $\{\boldsymbol{V}_i^{n+1}; \boldsymbol{\Omega}_i^{n+1}\}$, which are the values that should be used when enforcing the surface slip profile $\boldsymbol{V}_i' = \boldsymbol{V}_i^{n+1}$ ($\boldsymbol{\Omega}_i' = \boldsymbol{\Omega}_i^{n+1}$). Therefore, we adopt an iterative solution, and as an initial guess, we use the particle velocities at the previous time step, i.e., $\boldsymbol{V}_i' = \boldsymbol{V}_i^n$ ($\boldsymbol{\Omega}_i' = \boldsymbol{\Omega}_i^n$). The updated total velocity field is now obtained using the following:

$$\boldsymbol{u}^{**} = \boldsymbol{u}^* + \left[\int_{t_n}^{t_n+h} \mathrm{d}s \, \boldsymbol{f}_{\mathrm{sq}} \right] \tag{50}$$

$$\begin{aligned} \left[\int_{t_n}^{t_n+h} \mathrm{d}s \, \boldsymbol{f}_{\mathrm{sq}} \right] = \boldsymbol{u}^* &+ \sum_{i=1}^{N} \varphi_i \left(\boldsymbol{V}_i' + \boldsymbol{\Omega}_i' \times \boldsymbol{r}_i + \boldsymbol{u}_i^s - \boldsymbol{u}^* \right) \\ &+ \sum_{i=1}^{N} \phi_i \left(\delta \boldsymbol{V}_i + \delta \boldsymbol{\Omega}_i \times \boldsymbol{r}_i \right) - \frac{h}{\rho} \nabla p_{sq} \end{aligned} \tag{51}$$

The second term on the right hand side of Eq. 51 imposes a slip velocity profile $\boldsymbol{u}^s$ at the surface of each of the squirmers where $\varphi_i \propto (1 - \phi_i) \left| \nabla \phi_i \right|$ is a smooth surface profile function that is non-zero only within the interface domain of the squirmer (normalized to have a maximum value of one), and zero everywhere else (the red arrows in Fig. 2). The third term adds a counter-flow entirely within the particle domain, such that local momentum conservation is preserved (the blue arrows in Fig. 2). Assuming rigid-body motion, with velocities $\delta \boldsymbol{V}_i$ and $\delta \boldsymbol{\Omega}_i$, this requires

$$\int \mathrm{d}\boldsymbol{x} \, \phi_i \left(\delta \boldsymbol{V}_i + \delta \boldsymbol{\Omega}_i \times \boldsymbol{r}_i \right) = - \int \mathrm{d}\boldsymbol{x} \, \varphi_i \left(\boldsymbol{V}_i' + \boldsymbol{\Omega}_i' \times \boldsymbol{r}_i + \boldsymbol{u}_i^s - \boldsymbol{u}^* \right) \tag{52}$$

$$\int \mathrm{d}\boldsymbol{x} \, \boldsymbol{r}_i \times \phi_i \left(\delta \boldsymbol{V}_i + \delta \boldsymbol{\Omega}_i \times \boldsymbol{r}_i \right) = - \int \mathrm{d}\boldsymbol{x} \, \boldsymbol{r}_i \times \varphi_i \left(\boldsymbol{V}_i' + \boldsymbol{\Omega}_i' \times \boldsymbol{r}_i + \boldsymbol{u}_i^s - \boldsymbol{u}^* \right) \tag{53}$$

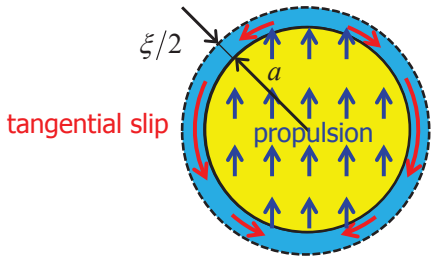

Figure 2. Schematic representation of the updating scheme used to enforce the slip boundary condition at the surface of the squirmers. Each particle is considered to exert a force on the fluid at the surface, in order to maintain the specified flow profile $\boldsymbol{u}^s$ (red arrows) for the squirming motion. To ensure local momentum conservation, a counter-flow is added within the particle domain (blue arrows).

from which we can easily obtain the counter-flow terms $\delta \boldsymbol{V}_i$ ($\delta \boldsymbol{\Omega}_i$) from the particle velocities $\boldsymbol{V}_i'$ ($\boldsymbol{\Omega}_i'$). A schematic representation of the procedure used to enforce the specific slip-boundary conditions for our model squirmers is shown in Fig. 2. Finally, the pressure term due to the squirming motion p_{sq} is obtained from the incompressibility condition $\nabla \cdot \boldsymbol{u}^{**} = 0$. At this point, the momentum conservation relation is solved for the total velocity field.

iii) The hydrodynamic force and torque exerted by the fluid on the colloids (which includes all contributions to the squirming motion) is again derived by assuming momentum conservation. The time integrated hydrodynamic force and torque for a period h are equal to the momentum exchange over the particle domain:

$$\left[\int_{t_n}^{t_n+h} \mathrm{d}s \, \left(\boldsymbol{F}_i^{\mathrm{H}} + \boldsymbol{F}_i^{\mathrm{sq}}\right)\right] = \int \mathrm{d}\boldsymbol{x} \, \rho \phi_i^{n+1} \left(\boldsymbol{u}^{**} - \boldsymbol{u}_p^n\right) \tag{54}$$

$$\left[\int_{t_n}^{t_n+h} \mathrm{d}s \, \left(\boldsymbol{N}_i^{\mathrm{H}} + \boldsymbol{N}_i^{\mathrm{sq}}\right)\right] = \int \mathrm{d}\boldsymbol{x} \, \left[\boldsymbol{r}_i^{n+1} \times \rho \phi_i^{n+1} \left(\boldsymbol{u}^{**} - \boldsymbol{u}_p^n\right)\right] \tag{55}$$

From this and any other forces on the colloids, the particles velocities are updated according to the following equations:

$$\boldsymbol{V}_i^{n+1} = \boldsymbol{V}_i^n + M_p^{-1} \left[\int_{t_n}^{t_n+h} \mathrm{d}s \, \left(\boldsymbol{F}_i^{\mathrm{H}} + \boldsymbol{F}_i^{\mathrm{sq}}\right)\right] + M_p^{-1} \left[\int_{t_n}^{t_n+h} \mathrm{d}s \, \left(\boldsymbol{F}_i^{\mathrm{C}} + \boldsymbol{F}_i^{\mathrm{ext}}\right)\right] \tag{56}$$

$$\boldsymbol{\Omega}_i^{n+1} = \boldsymbol{\Omega}_i^n + \boldsymbol{I}_p^{-1} \cdot \left[\int_{t_n}^{t_n+h} \mathrm{d}s \, \left(\boldsymbol{N}_i^{\mathrm{H}} + \boldsymbol{N}_i^{\mathrm{sq}}\right)\right] + \boldsymbol{I}_p^{-1} \cdot \left[\int_{t_n}^{t_n+h} \mathrm{d}s \, \boldsymbol{N}_i^{\mathrm{ext}}\right] \tag{57}$$

We recall that we have imposed the slip profile $\boldsymbol{u}^s$ with respect to the primed velocities $\{\boldsymbol{V}_i'; \boldsymbol{\Omega}_i'\}$, which need not be equal to the final velocities of the particle at step $n+1$. To maintain consistency, we iterate over Eqs. 50-57 until a convergence of velocities is achieved.

iv) Finally, the resulting particle velocity field $\phi^{n+1}\boldsymbol{u}_p^{n+1}$ is enforced over the total velocity field using the following relations:

$$\boldsymbol{u}^{n+1} = \boldsymbol{u}^{**} + \left[\int_{t_n}^{t_n+h} \mathrm{d}s\, \phi \boldsymbol{f}_p\right] \tag{58}$$

$$\left[\int_{t_n}^{t_n+h} \mathrm{d}s\, \phi \boldsymbol{f}_p\right] = \phi^{n+1}\left(\boldsymbol{u}_p^{n+1} - \boldsymbol{u}^{**}\right) - \frac{h}{\rho}\nabla p_{\mathrm{p}} \tag{59}$$

wherein the pressure due to the rigidity constraint obtained from the incompressibility condition $\nabla \cdot \boldsymbol{u}^{n+1} = 0$. The total pressure field is then given by $p = p^* + p_{\mathrm{p}} + p_{\mathrm{sq}}$.

The above procedure defines the consistent time-propagation, $\{\boldsymbol{u}^n; \boldsymbol{R}_i^n, \boldsymbol{Q}_i^n, \boldsymbol{\Omega}_i^n\} \rightarrow \{\boldsymbol{u}^{n+1}; \boldsymbol{R}_i^{n+1}, \boldsymbol{Q}_i^{n+1}, \boldsymbol{\Omega}_i^{n+1}\}$, to simulate self-propelled squirmers in incompressible fluids.

We are aware of two alternative simulation methods that aim to describe these squirmer suspensions at the same level of description, the first was developed by Ramachandran et al.[35] using a Lattice Boltzmann model, and the second was originally introduced by Downton and Stark[36] within a multi-particle collision dynamics framework, and later extended by Götze and Gompper[37] to recover the correct rotational dynamics. For the moment though, these DNS approaches have not been extensively used to study these types of swimming systems; the most popular methods, which still account for the hydrodynamic interactions, have usually been based on Stokesian Dynamics[31,34], and are thus limited to Newtonian fluids in the Stokes regime.

5 Concluding Remarks

A new computational method named the SPM has been developed to simulate particle dispersion in fluids[4–21]. Utilizing a smoothed profile for particle-fluid boundaries, hydrodynamic interactions in many particle dispersions can be fully taken into account, yielding both accurate and efficient results. In principle, the SPM can be easily applied to systems consisting of many particles with different shapes. The reliability and the performance of the method was confirmed to be satisfactory by several critical tests[4–22].

Recently, we extended the SPM to particle dispersions in compressible fluids[18]. The validity of the method was confirmed by calculating the velocity relaxation function of a single spherical particle in a compressible fluid[21]. The effect of compressibility on the velocity relaxation was also observed, revealing a two-stage relaxation process for low-compressibility fluids and a backtracking motion for high-compressibility fluids. A simulation of the motion of a single spherical particle in a fluctuating fluid was also performed. The calculated velocity autocorrelation function of the particle showed good agreement with the analytical solution of the relaxation function, thereby confirming the validity of the fluctuation-dissipation theorem without any fitting parameters.

We have also shown that SPM can be extended to systems with self-propelled swimming particles, making it possible to describe the actions of squirmers (active swimmers that move due to self-generated surface tangential velocities)[21]. The validity of the method was confirmed by comparing the simulation data with the exact results for the case of a

single swimmer, wherein the correct swimming speed is recovered and it is possible to accurately reproduce the fluid flow generated by the squirming motion. The advantage of the SPM for swimming particles in comparison with Stokesian Dynamics (which have been successfully and extensively used to study these systems)[31,34] is its applicability to particle dispersions in complex fluids. This is relevant in the case of swimming micro-organisms as the role of nutrients and the presence of a non-Newtonian host fluid must be considered when making comparisons with experimental data.

Acknowledgements

The authors would like to express their gratitude to Dr. K. Kim, Dr. Y. Nakayama, Dr. T. Iwashita, and Dr. H. Kobayashi for their contributions to the development of the SPM. This work was supported by Grant No. KAKENHI 23244087.

References

1. J. F. Brady and G. Bossis, Ann. Rev. Fluid Mech., **20**, 111 (1988).
2. H. H. Hu, N. A. Patankar, M. Y. Zhu, J. Comput. Phys., **169**, 427 (2001).
3. K. Ichiki, J. Fluid Mech., **452**, 231 (2002).
4. `http://www-tph.cheme.kyoto-u.ac.jp/kapsel/`
5. R. Yamamoto, Phys. Rev. Lett., **87**, 075502 (2001).
6. Y. Nakayama and R. Yamamoto, Phys. Rev. E, **71**, 036707 (2005).
7. K. Kim, Y. Nakayama, and R. Yamamoto, Phys. Rev. Lett., **96**, 208302 (2006).
8. R. Yamamoto, K. Kim, Y. Nakayama, K. Miyazaki, and D. R. Reichman, J. Phys. Soc. Japan, **77**, 084804 (2008).
9. T. Iwashita, Y. Nakayama, and R. Yamamoto, J. Phys. Soc. Japan, **77**, 074007 (2008).
10. Y. Nakayama, K. Kim, and R. Yamamoto, Eur. Phys. J. E, **26**, 361–368 (2008).
11. T. Iwashita and R. Yamamoto, Phys. Rev. E, **80**, 061402 (2009).
12. T. Iwashita and R. Yamamoto, Phys. Rev. E, **79**, 031401 (2009).
13. T. Iwashita, Y. Nakayama, and R. Yamamoto, Progress of Theoretical Physics, **11**, 86–91 (2009).
14. T. Iwashita, T. Kumagai, and R. Yamamoto, Eur. Phys. J. E, **32**, 357–363 (2010).
15. H. Kobayashi and R. Yamamoto, Phys. Rev. E, **81**, 041807 (2010).
16. S. Jafari, R. Yamamoto, and M. Rahnama, Phys. Rev. E, **83**, 026702 (2011).
17. H. Kobayashi and R. Yamamoto, Phys. Rev. E, **84**, 051404 (2011).
18. R. Tatsumi and R. Yamamoto, Phys. Rev. E, **85**, 066704 (2012).
19. Y. Matsuoka, T. Fukasawa, K. Higashitani, and R. Yamamoto, Phys. Rev. E, **86**, 051403 (2012).
20. A. Hamid and R. Yamamoto, J. Phys. Soc. Japan, in print.
21. J. J. Molina, Y. Nakayama, and R. Yamamoto, arXiv:1212.6133.
22. X. Luo, M. R. Maxey, and G. E. Karniadakis, J. Comp. Phys., **228**, 1750 (2009).
23. M. Fujita and Y. Yamaguchi, Phys. Rev. E, **77**, 026706 (2008).
24. F. B. Usabiaga, I. Pagonabarraga, and R. Delgado-Buscalioni, J. Comp. Phys., **235**, 701–722 (2012).
25. F. B. Usabiaga, R. Delgado-Buscalioni, B. E. Griffith, A. Donev, arXiv:1212.6427.

26. L. D. Landau and E. M. Lifshitz, *Fluid Mechanics*, (Pergamon Press, London, 1959).
27. G. Erlebacher, M. Y. Hussaini, H. O. Kreiss, and S. Sarkar, Theor. Comput. Fluid. Dyn., **2**, 73 (1990).
28. J. V. José and E. J. Saletan, *Classical Dynamics: A Contemporary Approach*, (Cambridge University Press, New York, 1998).
29. M. J. Lighthill, Ann. Rev. Fluid Mech., **1**, 413–446 (1969).
30. J. R. Blake, J. Fluid Mech., **46**, 199–208 (1971).
31. T. Ishikawa, M. P. Simmonds, and T. J. Pedley, J. Fluid Mech., **568**, 119–160 (2006).
32. L. Zhu, E. Lauga, and L. Brandt, Phys. Fluids, **24**, 051902 (2012).
33. W. B. Russel, D. A. Saville, and W. R. Schowalter, *Colloidal Dispersions*, (Cambridge University Press, Cambridge, 1992).
34. J. W. Swan, J. F. Brady, R. S. Moore, and ChE 174, Phys. Fluids, **23**, 071901 (2011).
35. S. Ramachandran, P. B. Sunil Kumar, and I. Pagonabarraga, Eur. Phys. J. E, **20**, 151 (2006).
36. M. T. Downton and H. Stark, J. Phys.: Condens. Matt., **21**, 204101 (2009).
37. I. Götze and G. Gompper, Phys. Rev. E, **82**, 041921 (2010).